HHS Public Access

Author manuscript

Glia. Author manuscript; available in PMC 2018 December 01.

Published in final edited form as:

Glia. 2017 December ; 65(12): 1990–2002. doi:10.1002/glia.23209.

Oligodendrocyte *RasG12V* Expressed in its Endogenous Locus Disrupts Myelin Structure Through Increased MAPK, Nitric Oxide, and Notch Signaling

Haley E. Titus[1,2], **Alejandro López-Juárez**[1,2], **Sadiq H. Silbak**[1], **Tilat A. Rizvi**[1], **Madeleine Bogard**[1], and **Nancy Ratner**[1,*]

[1]Division of Experimental Hematology and Cancer Biology, Cincinnati Children's Hospital Medical Center, Cincinnati, OH, 45229, USA

Abstract

Costello syndrome (CS) is a gain of function Rasopathy caused by heterozygous activating mutations in the *HRAS* gene. Patients show brain dysfunction that can include abnormal brain white matter. Transgenic activation of *HRas* in the entire mouse oligodendrocyte lineage resulted in myelin defects and behavioral abnormalities, suggesting roles for disrupted myelin in CS brain dysfunction. Here we studied a mouse model in which the endogenous *HRas* gene is conditionally replaced by mutant *HRasG12V* in mature oligodendrocytes, to separate effects in mature myelinating cells from developmental events. Increased myelin thickness due to decompaction was detectable within one month of *HRasG12V* expression in the corpus callosum of adult mice. Increases in active ERK and Nitric Oxide (NO) were present in *HRas* mutants and inhibition of NO synthase (NOS) or MEK each partially rescued myelin decompaction. In addition, genetic or pharmacologic inhibition of Notch signaling improved myelin compaction. Complete rescue of myelin structure required dual drug treatments combining MAPK, NO or Notch inhibition; with MEK + NOS blockade producing the most robust effect. We suggest that individual or concomitant blockade of these pathways in Costello syndrome patients may improve aspects of brain function.

Keywords

Myelin; Rasopathy; Notch; Ras; Nitric Oxide; Costello Syndrome; Oligodendrocyte

Introduction

Rasopathies are genetic disorders in which patients are heterozygous for germline mutations in genes of the Ras-MAPK signaling pathway (Tidyman and Rauen 2016). Costello syndrome (CS) is a rare gain of function Rasopathy caused by a heterozygous mutation of

[*]**Corresponding Author**: Nancy Ratner, Nancy.Ratner@cchmc.org, Mailing address: 3333 Burnet Ave., Cincinnati Children's Hospital, Cincinnati, OH, 45229-7013, Telephone: 513-636-9469, Fax: 513-803-1083.

[2]These authors contributed equally to this work.

Author Contributions: H.T.M. and A.L.J. performed experiments, analyzed data, and drafted the manuscript. T.R. assisted with perfusions. S.H.S. and M.B. quantified g-ratios and myelin decompaction from electron micrographs; S.H.S. also performed statistical analyses. N.R. designed the project, aided in data analysis and interpretation, and edited the manuscript and figures.

the *HRAS* gene on chromosome 11p15.5, which results in neurocognitive impairment and relative macrocephaly (Quezada and Gripp 2007). Other manifestations include facial dysmorphism, growth retardation, gastrointestinal, skin and musculoskeletal anomalies, cardiovascular abnormalities, and tumor predisposition. Most CS patients show *HRASG12S* mutation, which causes psychomotor delay with low intelligence and developmental index scores (Zampino et al. 2007). Furthermore, a rare *HRASG12V* mutation was linked to a severe form of CS (Aoki et al. 2005). All these mutations increase HRAS-GTP and activation of downstream signals, including activation of the MAPK signaling pathway that results in phosphorylation of the kinases MEK1/2 and ERK1/2 (Quezada and Gripp 2007). Correlating with severe patient phenotypes, the *G12V* mutant of *HRAS* displays the lowest GTPase activity among known *HRASG12* mutations (Colby et al. 1986), and is a predominant mutation in human cancers (Aoki et al. 2005).

Mental retardation, macrocephaly and variable cognitive delay are frequent in CS patients (Axelrad et al. 2007; Gripp et al. 2010; Rauen 2007). Moreover, synaptic plasticity may be affected in CS patients (Mainberger et al. 2016). At cellular level, brain neurons and astrocytes have been studied in models of CS. Increased HRAS-GTP promotes production of cortical neurons with morphological deficits (Rooney et al. 2016). Human induced pluripotent stem cells from *RASG12S* CS patients differentiate to astroglia more rapidly than wild type cells. Additionally, *RASG12S* cells show abnormal astrocyte-to-neuron signaling, as do astrocytes in an astrocyte-driven *RASG12V* mouse model (Krencik et al. 2015). Interestingly, MRI studies have shown brain white matter (WM) abnormalities in CS patients, suggesting that delayed myelination and/or abnormal myelin contribute to CS developmental delays (Delrue et al. 2003). These studies, together with research relating defective oligodendrocyte function with mental illness (Haroutunian et al. 2014), suggest that hyperactive RAS in myelinating cells may contribute to CS pathology.

Myelin sheaths are plasma membrane projections of oligodendrocytes that spirally wrap axons and myelin layers become compacted, increasing axon conduction velocity (Bauer et al. 2009; Franklin and Gallo 2014). The Ras-MAPK pathway kinases MEK and ERK regulate several aspects of developmental, injury-induced and *in vitro* oligodendrogenesis as well as regulate the number of myelin wraps produced by normal oligodendrocytes (Fyffe-Maricich et al. 2011; Fyffe-Maricich et al. 2013; Guardiola-Diaz et al. 2012; Ishii et al. 2013; Xiao et al. 2012). In contrast, mice expressing the Ras-activating *HRasG12V* allele in cells of the oligodendrocyte lineage starting at embryonic day 12.5, exhibit myelin decompaction at intraperiod lines in adult mice. These mutants show hyperactive behavior and increased response to startle, correlating with the presence of abnormal myelin (Mayes et al. 2013). These results are consistent with the hypothesis that defects in myelinating cells contribute to phenotypes in Rasopathies.

Elevated Ras signaling through MEK/ERK can increase reactive oxygen and nitrogen species (ROS) (Heimfarth et al. 2013), and in *CNPase;HRasG12V* mice, nitric oxide (NO) mediates myelin decompaction (Mayes et al. 2013); *HRasG12V*-expressing white matter showed elevated NO synthases (NOS) and ROS, and blockade of NOS rescued aberrant behavior and myelin compaction. NO signaling inhibition also rescued myelin decompaction caused by inactivation of the Ras-GTP inhibitor *Nf1* in oligodendrocytes and, interestingly,

blocking NO production rescued abnormally hyperactive Notch signaling (López-Juárez et al. 2017). Cell-cell interactions through Notch signaling negatively regulate oligodendrocyte maturation and myelin wrapping (Wang et al. 1998; Watkins et al. 2008). While a direct link between RAS and Notch in mOLs has not been identified, in other systems multiple levels of crosstalk between these signaling pathways are known (Sundaram 2005). Ras-GTP can act upstream of Notch signaling and the Notch pathway can feedback to antagonize the Ras pathway (Baumgart et al. 2015). Here, we aimed to delineate effects downstream of *HRasG12V* mutation in mature oligodendrocytes (mOLs).

A limitation of transgenic *HRasG12V* mice to model the CS brain is that transgenic expression of activated *RAS* often fails to accurately model disease, due to altered levels, timing and/or strength of activating alleles in specific cell types (Di Nicolantonio et al. 2008; Sarkisian et al. 2007; To et al. 2008). For example, *CNPase;HRasG12V* was expressed early in development, in immature and mature oligodendrocytes, and lacks normal genomic regulation (Mayes et al. 2013). To better mimic human *HRasG12V* mutation in CS, we conditionally substituted the endogenous wild type *HRas* with the mutant *HRasG12V* (Chen et al. 2009) in mature oligodendrocytes (mOLs). We found that myelin decompaction occurs rapidly after oligodendrocyte *HRasG12V* hemizygous expression. Compaction is improved by individual inhibition of signal pathways and is fully rescued by combined inhibition of MEK and NOS.

Materials and Methods

Mouse Husbandry

All mouse studies were approved by The Cincinnati Children's Hospital Research Foundation, Institutional Animal Care and Use Committee (IACUC). Mice were housed in a temperature- and humidity- controlled vivarium on a 12-hour light-dark cycle with free access to food and water. Adult (<8 weeks old) male and female mice were used for experimentation.

Mouse Strains

See description in table below. All mice were maintained on a C57Bl/6 background. Mice were genotyped by PCR as previously described (references).

Tamoxifen Injections

Tamoxifen (Sigma-Aldrich) (100 μL; ~75mg/kg of body weight) in sunflower seed oil was administered I.P. twice daily for 4 consecutive days. Treatment was performed at 8 week of age in littermate WT and mutant mice, of both sexes. No genotype- or sex-dependent changes in body weight were observed.

Tissue Processing

Mice were anesthetized and perfused with 0.9% saline followed by ice cold 4% paraformaldehyde. Tissues were removed, post-fixed in 4% paraformaldehyde overnight and sectioned using a vibratome (Leica) or transferred to 20% sucrose for subsequent frozen sectioning.

Immunohistochemistry and Antibodies

Cryostat or vibratome sections were processed for immunohistochemistry using antibodies for markers; Rabbit anti-pERK (1:200; Cell Signaling) and Mouse anti-APC (CC1 1:300, Calbiochem). Fluorescent secondary antibodies (donkey anti-rabbit conjugated to Cy3 and donkey anti-mouse conjugated to Cy5, Invitrogen, Carisbad, CA) were used at 1:300 dilution. Fluoromount G was used to mount fluorescent sections.

Image Analysis

Fluorescent images were captured on a Nikon C2 Confocal microscope using a 20× objective (2× Zoom for 40×) with lasers (405, 488, 561). Cell counting was performed using an ImageJ micromanager plugin and Imaris Software.

Electron Microscopy

Wild type and experimental littermate mice were processed at the same time to minimize myelin structure artifacts caused in processing. Mice were perfused with 4% paraformaldehyde/2.5% glutaraldehyde and post–fixed in the same fixative overnight. The corpus callosum was dissected and transferred to 0.175M cacodylate buffer, osmicated, dehydrated and embedded in Embed 812 (Ladd Research Industries). Ultrathin sections were stained in uranyl acetate and lead citrate, and then imaged on a Hitachi Model H-7600 transmission electron microscope.

Myelin Analysis

To quantify total decompaction, myelin sheaths were rated as compacted or decompacted, as defined by the presence or absence of fibers with disruption of the myelin sheath (i.e. decompacted = presence of areas with splitting of myelin lamellae). To measure severity of decompaction, we analyzed each quartile of each fiber (4 measurements per myelinated axon cross section), and report results as 1, 2, 3, or 4 quadrants showing decompaction (color coded in figures 3–6). The g-ratio of myelinated fibers was obtained by dividing the diameter of each axon by the fiber diameter (300–500 axons/mouse, n=3–5 mice/genotype/condition), using ImageJ software. When a fiber was identified as compact, or showed 4 quadrants decompacted, 1 measurement was collected for g-ratio. However, if a fiber showed 2 quadrants decompacted, then 2 measurements were collected, perpendicular to each other; if a fiber showed 1 or 3 quadrants decompacted, 4 measurements at 90° angles were collected for measurement of myelin thickness. Measurement was carried out by individuals blinded to sample identify and treatment.

Flow Cytometry

Adult murine brains were processed for flow cytometry as described (Robinson et al. 2014). Flow cytometry was performed using FacsDiva software for acquisition on an LSR II flow cytometer. We used antibodies recognizing oligodendrocyte progenitors (PDGFRα 1:50; Millipore), and mature oligodendrocytes (GalC 1:100; Millipore). An ENZO Life Sciences kit was used to detect Nitric Oxide (ENZ-51013-200). Importantly, a positive control (L-arginine, a nitric oxide synthase substrate) and a negative control (C-PTIO, a nitric oxide scavenger) validated staining specificity for nitric oxide (Kalyanaraman et al. 2012).

Analysis was performed using FlowJo10 software. Compensation was carried out using positive and negative controls, as well as Fluorescence Minus One (FMO) samples, which were dissociated forebrain cells incubated with all stains except the marker of interest, to allow for appropriate compensation.

Drug Treatments

Gamma secretase inhibitor (GSI; MRK-003) was prepared fresh weekly and dosed at 300 mg/kg in 0.5% methocel by oral gavage (Lewis et al. 2007; Sparey et al. 2005). For histology, we dosed mice once weekly for 4 weeks, and sacrificed them 6 hours after the last dose (n=5 doses). Fresh solution of L-NG-Nitroarginine Methyl Ester (L-NAME) at 0.4mg/kg (100μM in 1× PBS) was administered daily. For pathology and flow analysis, mice were injected intraperitoneally (IP) daily with 100μL for 7 days and sacrificed 6 hours after the last dose. MEK inhibitor (PD0325901 from Pfizer) was made fresh weekly and dosed at 1.5 mg/kg in 0.5% methocel/0.2% Tween 80 by oral gavage. For histology, we dosed mice every day for 3 weeks.

Statistical Analysis

The minimal number of independent experiments/mice per statistically significant experiment was 3. Comparison between two groups used Student's t-tests with significance cutoff of $p<0.05$. For comparison of three or more groups, one-way ANOVA followed by Tukey post hoc test with significance cutoff of $p<0.05$. Linear regression of g-ratio vs. axon diameter was performed using Graph Pad software.

Results

RasG12V Mutation in Mature Oligodendrocytes Activates MAPK Signaling Without Affecting Oligodendrocyte Numbers

To study how the CS mutation *HRasG12V* affects myelinating mOLs, we induced the expression of *HRasG12V* from the *Ras* endogenous locus. Mice carrying the mutant allele *HRasG12V* downstream of the endogenous *HRas* gene flanked by *loxP* sites (Chen et al. 2009) were crossed with mice carrying a tamoxifen-inducible Cre recombinase under the transcriptional regulatory elements of proteolipid protein 1 (*Plp1Cre^{ERt2}*) (Doerflinger et al. 2003). In these mice, tamoxifen treatment induces the expression of *HRasG12V* upon excision of the endogenous *HRas* (Fig. 1A). Recombination using this *PlpCre* driver targets ~35% of mOLs in the corpus callosum (CC), and essentially no NG2$^+$ oligodendrocyte progenitors or GFAP$^+$ astrocytes are recombined (Koenning et al. 2012; Mayes et al. 2013). Numerous studies indicate that diverse phenotypes are caused by varying levels of Ras-MAPK activation (Cox and Der 2003; Serrano et al. 1997). With respect to myelin defects, decreasing gene-dose of *Nf1,* a negative regulator of Ras, correlates with progressively increasing levels of decompaction (López-Juárez et al. 2017); therefore, we studied both *HRasG12V* homozygous and hemizygous mutants. Adult (>8 week old) hemizygous *PlpCre^{ERt2};HRas$^{G12V/+}$* (henceforth *pRsG/+*) and homozygous *PlpCre^{ERt2};HRas$^{G12V/G12}$* (henceforth *pRsG/G*) *RasG12V* mutants, as well as control *PlpCre^{ERt2}* or *Ras$^{G12V/+}$* littermates, were treated with tamoxifen, and analysis of the CC at different time points was performed. No phenotypic differences were observed between control *PlpCre^{ERt2}* and

pRas$^{G12V/+}$ mice (henceforth referred as wild type; WT) and, in agreement with a previous report (Doerflinger et al. 2003), we did not observe spontaneous activity of *PlpCre*^{ERt2}. We confirmed Ras hyper-activation specifically in mOLs by assessing the presence of the phosphorylated form of ERK (pERK), a downstream target of Ras-GTP, in cells stained with the mOL marker CC1 (Fig. 1B). The number of CC1$^+$ mOLs in the CC of *RasG12V* mutants was not significantly different from that in WT mice (Fig. 1C). In contrast, significantly increased numbers of pERK$^+$CC1$^+$ mOLs were detected *in pRsG/G* and *pRsG/+* mutants 1 month after tamoxifen treatment (Fig. 1D). We note that high variability in the number of the pERK$^+$;CC1$^+$ mOLs occurred in homozygous *RsG12V* mutants, yet specific induction of hyperactive Ras was achieved in both Ras mutants.

Constitutive *HRas* Activation in Mature Oligodendrocytes Decreases g-ratio

To study WM abnormalities after Ras activation, we analyzed the ultrastructure of axons and myelin in sagittal sections at the midline of the CC of *RasG12V* mutants using electron microscopy (Fig. 2A). Unbiased counting of myelinated axons revealed significantly decreased g-ratio in *pRsG/+* and *pRsG/G* mutants 1 month post-tamoxifen treatment, as compared to WT mice (Fig. 2B). We did not count numbers of small unmyelinated axons; however, numbers of large caliber unmyelinated axons in the CC did not change with genotype (n= 3 mcie/genotype, one-way ANOVA p=0.057, with Tukey's multiple comparison test WT vs, *pRsG/+; 0.072;* WT *vs,* pRsG/G; p=0.093). Further, decreases in g-ratio were observed in both mutants at 6 months post-tamoxifen (Fig. 2B), indicating that the decrease in g-ratio is progressive. One month post tamoxifen, low g-ratio was not preferentially associated to small or large diameter axons, as indicated by linear regression analysis of g-ratio vs. axon diameter in mutant vs WT mice (Fig. 2C). However, at six months post-tamoxifen, an increased association of low g-ratio with small caliber axons was observed in both homozygous and hemizygous *HRasG12V* mutants as compared to WT mice (Fig.2D); indicating that small caliber axons contribute to progressive abnormal g-ratio, and/or axons shrink over time (Fig. 2B). Myelinating cells regulate axon caliber (Cole et al. 1994; Colello et al. 1994), so myelin defects caused by *HRas* activating mutation in mOLs might disrupt axon structure. In fact, quantification of myelinated axon diameter indicated a significant skew to decreased axon diameter in both *pRsG/+* and *pRsG/G* mutants, as compared to WT (Fig. 2E). As neurons whose axons project through the CC do not express the *PlpCre* allele (Koenning et al. 2012; Mayes et al. 2013), change in axon diameter is likely to be secondary to disturbed myelin integrity (Cole et al. 1994; Colello et al. 1994), thus we focused on the analysis of the myelin structure.

Hyperactivation of *HRas* in Mature Oligodendrocytes Results in Myelin Decompaction

The MAPK signaling pathway regulates numbers of myelin wraps as well as compaction of myelin in mOLs (Ishii et al. 2013, López-Juárez et al. 2017). We observed that myelin thickness was increased in *RasG12V* mice, as both homozygous and hemizygous mutants displayed myelin decompaction at intraperiod lines (Fig. 2A, arrows), without showing changes in the number of myelin lamellae wrapping axons (Fig. 3A). Therefore, the two parameters determining g-ratio, axon diameter and myelin thickness, were abnormal in *HRas* mutants. Quantification of the fibers showing decompaction indicated a significant increase in the percent of myelin sheaths with decompaction in both *RasG12V* mutants 1

month after tamoxifen treatment, as compared to WT mice (Fig. 3B). This phenotype was sustained for at least 6 months post-tamoxifen with no obvious worsening of decompaction. To determine changes in the severity of myelin decompaction, we divided myelinated fibers into quadrants and reported the percent of fibers showing decompaction in 1, 2, 3 or 4 quadrants around each axon. We corroborated similar decompaction patterns in both *RasG12V* mutants over time (Fig. 3B, bottom; color code). Thus, hyperactivation of HRas in mOLs disrupts myelin structure within 1 month, and this phenotype is sustained, while the non-cell-autonomous effects on axons appear progressive. Next, we analyzed whether small or large diameter axons preferentially show myelin decompaction. As shown in figure 3C, small myelinated axons (<0.9 μm) of homozygous and hemizygous *HRas* mutants, and medium caliber myelinated axons (0.91 – 1.2 μm) of homozygous mutants, were affected by myelin decompaction 1 month post-tamoxifen. These results indicate that myelin decompaction impacts small caliber axons in the short-term and may cause axon shrinkage over time (Fig. 2B–E). As hemizygous *HRasG12V* mutation most closely models CS patients, we focused additional study on the analysis of signaling pathways controlling myelin decompaction in *pRsG/+* mutants.

Myelin Decompaction is Partially Rescued by Inhibition of MEK or NOS, and Full Rescue is Achieved by the Concomitant Treatment in Hemizygous *HRas* Mutants

In order to gain insight into molecular mechanisms driven by HRas activating mutations that affect oligodendrocytes, we first evaluated the effect of blocking MEK, the major effector pathway downstream of Ras-GTP in Rasopathies. We analyzed myelinated fibers in the CC of mice treated with the blood brain barrier-permeable MEK inhibitor (MEKi) PD0325901, starting 1 month post-tamoxifen (Barrett et al. 2008). Administration of MEKi did not significantly change myelin decompaction in WT mice, although a trend toward increased decompaction was observed (Fig. 4A). Likewise, no differences in g-ratio were observed between vehicle-treated WT and MEKi-treated mice (Fig. 4B). MEKi treatment slightly improved compaction in *pRsG/+* mutants, as compared to vehicle-treated mutants, but this was not significant (Fig. 4A). In contrast, MEKi significantly normalized g-ratio in *pRsG/+*, however full recovery to WT levels was not achieved (Fig. 4B). These results indicate that MEKi, at a therapeutically relevant dose, does not fully rescue myelin defects caused by *HRasG12V* in mOLs. We therefore searched for additional effectors downstream of Ras.

It was previously reported that myelin defects resulting either from activation of *HRas* in the oligodendrocyte lineage, or from inactivating the Ras regulator *Nf1* in mOLs, can be partially rescued by blocking the production of Nitric Oxide *in vivo* (López-Juárez et al. 2017; Mayes et al. 2013). Therefore, we first tested whether NO signaling is abnormally increased in *pRsG/+* mutants at a time point when myelin defects are evident. We dissociated cells from the forebrain of WT and *pRsG/+* mice and stained them with cell-type markers as well as a dye that emits fluorescence in the presence of NO. Flow cytometry analysis revealed that the number of $GalC^+$ mOLs showing staining for NO dye was significantly increased in the *pRasG12V* mutants as compared to WT mice, while the number of $PDGFRa^+;NO^+$ oligodendrocyte precursors remained unchanged (Fig. 4C). Therefore, we evaluated myelin defects in *pRasG12V* hemizygous mutants treated with L-NAME, an inhibitor of NO synthases, starting at 1 month post-tamoxifen. L-NAME

treatment caused a significant decrease in the number of fibers with decompaction in the CC of *pRsG/+* mice (Fig. 4A) and a significantly increased g-ratio (Fig. 4B), as compared to vehicle-treated Ras mutants. However, neither myelin compaction nor g-ratio were fully restored to WT levels.

To determine whether the combination of NOS and MEK inhibition provides an additive benefit, we assessed myelin properties in *pRsG/+* mutants treated with MEKi and L-NAME and found that pathologic myelin decompaction was abolished (Fig. 4A). In fact, under these conditions, myelin was more compact than in untreated WT CC, and g-ratio was increased over the levels observed in WT mice (Fig. 4B); suggesting that basal MAPK-NO signaling contributes to the maintenance of normal compact myelin. Taken together, these data show that disturbed MAPK and NO signaling cooperate to disrupt myelin structure upon *HRasG12V* expression.

Inhibition of Notch Signaling Rescues Myelin Defects in Hemizygous *HRasG12V* Mutants

We recently reported that myelin defects in a model of NF1 Rasopathy result in part from abnormal hyper-activation of Notch in mOLs, and that mice overexpressing the Notch Intracellular Domain (the active form of Notch that translocates to the nucleus) show disrupted myelin compaction and a reduced g-ratio (López-Juárez et al. 2017). Therefore, we hypothesized that myelin abnormalities in *pHRasG12V* mutants may also require Notch activation. We used the tamoxifen-inducible allele *Rbpjfl/fl* to inactivate recombining binding protein suppressor of hairless (RBPJ), the essential transcriptional co-factor for canonical Notch signaling, in *pRsG/+* mutants. Analysis of myelinated axons in the CC of $PlpCre^{ERt2};HRas^{G12V/+};Rbpj^{fl/fl}$ (henceforth *pRsG/+;pRBPJ*) mutants showed only a trend toward a decrease in the percent of decompacted fibers at 1 month post-tamoxifen treatment, versus *pRsG/+* mutants (Fig. 5A). Similarly, no significant differences were found between the g-ratio of *pRsG/+;pRBPJ* and *pRsG/+* mutants (Fig. 5B).

Upon Notch ligand binding, active NICD is released by the action of Gamma secretase. Therefore, inhibition of this enzyme prevents Notch signaling. As a secondary strategy to evaluate the Notch pathway contribution to abnormal myelin in *pRasG12V* mutants, we treated mice with Gamma secretase inhibitor (GSI). Analysis of CC myelinated axons revealed a significant decrease in the number of fibers with decompaction (Fig. 5C) and an increase in g-ratio (Fig. 5D) in GSI-treated *pRsG/+* mutants as compared to vehicle-treated *pRsG/+* mice. Although the rescue of the phenotypes was not to the level of WT mice, these data support participation of Notch signaling downstream of *RasG12V* mutation. The different level of rescue observed in *RBPJ* loss model and GSI treatment (compare Fig. 5A–C and 5B–D) may include compensation for the absence of RBPJ in mOLs, GSI effects on cells in addition to mOLs, and/or effects of GSI on other γ-secretase substrates (Langosch et al. 2015).

Concomitant Inhibition of Notch Signaling and MAPK or NO Signal Pathways Fully Rescues Myelin Abnormalities in *HRasG12V* Mutants

Given that neither treatment with MEKi, nor treatment with L-NAME, fully rescued myelin compaction in *pRsG/+* mutants, and that blocking both pathways fully rescued the

phenotypes, we tested whether inhibition of Notch pathway lead to additive effects on myelin structure. We evaluated myelinated axons in the CC of *pRsG/+;pRBPJ* double mutants after treatment with MEKi or L-NAME. The combination of inducible genetic Notch inactivation with MEKi treatment decreased myelin decompaction significantly, to levels observed in WT mice (Fig. 6A). Fiber g-ratio was significantly improved in *pRsG/+;pRBPJ* double mutants treated with MEKi as compared to vehicle-treated mice of the same genotype (Fig. 6B). However, this combination did not improve g-ratio more than MEKi treatment alone, possibly because non-cell autonomous effects on axon diameter are not affected by *pRBPJ* mutation in mOLs (Fig. 2C).

Additionally, *pRsG/+;pRBPJ* double mutant mice treated with L-NAME showed improved myelin compaction (Fig. 6C). Furthermore, g-ratio improved to WT levels (Fig. 6D). Overall, these data support the idea that myelin decompaction caused by increased levels of Ras-GTP can be restored through use of combinations of drugs targeting MAPK, NO, and/or Notch. However, rescue of g-ratio occurs only with the combination of drugs targeting both MAPK and NO. Taken together, our results suggest that pharmacological tools targeting MAPK, NO, and/or Notch signal pathways, alone or in combinations, may ameliorate CNS manifestations in Costello Syndrome.

Discussion

RAS regulators, RAS effectors, and RAS proteins themselves can be mutated in Rasopathies and are the subject of intensive research, with new mutations still being detected (Tidyman and Rauen 2016). Precisely how increases in active RAS-GTP impair brain function is still poorly understood. In CS, as in many Rasopathies, hyperactive Ras signaling can cause neurodevelopmental abnormalities, including cognitive impairment, autism spectrum disorders, and white matter abnormalities. Here we report that the Ras-activating mutation *HRasG12V,* conditionally expressed in the endogenous *H-Ras* locus, causes pathological myelin decompaction mediated by MAPK, Nitric Oxide, and Notch signaling.

Strong evidence supports the idea that overexpression of mutant RAS can result in altered localization and cellular responses, versus RAS-GTP activated physiologically (Di Nicolantonio et al. 2008; Quinlan et al. 2008; Sarkisian et al. 2007). This is thought to result because local regulatory elements control *RAS* expression and downstream effects within tissues (To et al. 2008). Therefore, use of the *HRasG12V* in its endogenous locus should accurately mimic cell autonomous effects of the Costello mutation in OL. Previously we reported myelin decompaction in a transgenic *CNP-HRasG12V* model, in which *HRasG12V* is expressed in developing OPCs and oligodendrocytes (Mayes et al. 2013). Our new study of *HRasG12V* induction in its endogenous locus in mOLs, confirms a role of hyperactive HRas in pathological myelin decompaction and, importantly, shows the onset of this phenotype in mature OLs of the adult mouse, rather than in developmental stages with lower potential for therapeutics. While *HRasG12V* is a rare mutation associated with severe manifestations in CS patients (Aoki et al. 2005), experimental *G12V* mutation mimicked phenotypes found in models of the most common *HRas* mutation (*G12VS*) (Rooney et al. 2016).

Several studies using gain and loss of function models have shown that the RAS effectors ERK1 and ERK2 promote the establishment and maintenance of myelin thickness, regulating both the number of myelin wraps and the abundance of major myelin proteins (Fyffe-Maricich et al. 2011; Fyffe-Maricich et al. 2013; Guardiola-Diaz et al. 2012; Ishii et al. 2013). In contrast, we show that *HRasG12V* expression in mOL causes myelin thickening due to pathological myelin decompaction, without an increase in the number of myelin lamellae. Myelin decompaction was also reported in the *CNP-HRasG12V* mouse model in which changes in expression of tight junction, not myelin, proteins were observed (Mayes et al. 2013). Differences in myelin phenotypes may be due to the mutants analyzed and their effects on levels of RAS activation. Mechanistically, Ras-GTP activation of ERK1/ERK2 activates feedback regulation that dampens or enhances Ras signaling (Rauch et al. 2016). For example, the Ras-MAPK negative regulator Sprouty 2, induced on growth factor stimulation through MAPK, is highly expressed in the brain, where it dampens the impact of MAPK pathway activation in germline-*HRasG12V* mutants. Strong activation of MEK/ERK is observed in the liver of the same mice, where Sprouty2 is virtually absent (Chen et al. 2009). This is important because high levels of Ras-MAPK activation mediate cell senescence and apoptosis, while lower levels alter cell proliferation and differentiation (Cox and Der 2003; Serrano et al. 1997). Therefore, differences in feedback regulation in cells with Ras activation differ from those with direct MEK/ERK activation. In addition, RAS-GTP activates multiple effector cascades parallel to MAPK activation, which may contribute to decompaction in Ras but not in MEK or ERK mutants.

Based on this and previous studies, maintenance of myelin compaction is controlled by Ras-MAPK. Thus, *HRasG12V* expression or *Nf1* mutation in mOLs causes decompaction in previously myelinated fibers (López-Juárez et al. 2017). However, once a maximum level of decompaction is reached (60–75% of total myelinated fibers), no further increase is observed over time. This result suggests that adhesion systems may maintain this residual compaction. Compact myelin proteins such as Claudin 11, proteolipid protein, and connexin 32 (Gielen et al. 2006; Martini and Schachner 1997) are likely to be involved. It is also possible that as-yet-unidentified signaling pathways contribute to maintaining myelin compaction. Additional phenotypes caused by *HRas* mutation in mOLs, such as axon caliber decrease, appear to be non-cell-autonomous effects and show slower progression.

We directly show elevated NO in *pRsG/+* mOLs, consistent with roles for Ras-NO signaling in the myelin decompaction phenotype and supporting the involvement of this signal downstream of *HRasG12V* expression. Notably, in CNP-*HRasG12V* mice behavioral abnormalities were rescued by blocking NO generation using L-NAME (Mayes et al. 2013). In *ex-vivo* brain preparations, Ras signaling through MEK/ERK also increased reactive oxygen/nitrogen species, and NO protected oligodendrocytes through inhibition of nitrotyrosine-induced ERK phosphorylation (Heimfarth et al. 2013). At higher levels, NO can be toxic; suppressing myelin gene transcription, translation of myelin proteins (Jana and Pahan 2013), and promoting apoptosis (Li et al. 2011). In *pRsG/+* mOLs, while inhibition of NO production decreased myelin decompaction, additionally targeting MEK was able to fully rescue the myelin phenotype. Why both inhibitors are necessary in *pRsG/+* mOLs remains unclear; it may result from vertical inhibition (e.g. the additive impact of blocking two members of the same signaling pathway) and/or from blocking pathway crosstalk.

In mOLs lacking the *Nf1* Rasopathy gene, thereby activating RAS-GTP, NO links MAPK and Notch signaling (López-Juárez et al. 2017). Our data support a role for Notch signaling in mOLs, but in *HRasG12V* mOL the evidence is less robust than for the *Nf1* model. Thus, while we demonstrate a trend toward improvement in myelin compaction in *HRasG12V* mice lacking *Rbpj*, the effect is not significant (unlike in the *Nf1* setting). Additionally, given that gamma secretase has at least 90 substrates, the effects of GSI, while significant, cannot be taken as specific to inhibition of Notch signals. Yet, *Rpbj* loss in *HRasG12V* mice, sensitized mutant cells to MEK or NOS inhibition, supporting the view that Notch signaling is relevant in this model. It may be that levels of active Notch in *HRasG12V* mice are low, and/or that feedback interaction between the Ras-MAPK and the Notch pathway occurs; possibly through decreasing activity of one increasing dependence on the other. In either event, our results indicate that Ras and Notch signals are involved in myelin compaction.

We observed consistent “more-than-complete” rescue of phenotypes following combinatorial drug treatments in *HRasG12V* hemizygous mutants. This effect was shown previously for myelin decompaction in *Nf1* and *CNP-HRas* mOL mice treated with inhibitors (López-Juárez et al. 2017; Mayes et al. 2013). This response could result from off target activity of pharmacological tools. We support the alternative explanation that combination treatments overshoot dose(s) needed for optimal rescue. If this is the case, expression of Rasopathy genes, including *HRasG12V,* uncover signaling pathways that maintain normal myelin compaction by balancing levels MAPK, NO and Notch. Relationships between MEK-NOS-Notch pathways controlling normal and pathological myelin in a cell-autonomous manner are likely to be complex, and future studies will need to consider titering levels of response to optimize inhibitor effects in specific settings. Furthermore, non-cell-autonomous activation of these pathways seems to add complexity to the system. Recombination is elicited by the *PlpCreER* driver in about 35% of mature carpus callosum oligodendrocytes (Koenning et al. 2012, Mayes et al., 2013). In contrast, decompaction is observed in ~60–70% of myelinated fibers, making it unlikely that only recombinant oligodendrocytes show abnormal myelin. In previous studies (Mayes et al. 2013, López-Juárez et al. 2017), as well as in this study, we show data supporting the idea that non-cell-autonomous effects are mediated at least in part by a diffusible signal, NO.

In summary, MEK, NOS, and gamma secretase inhibitors each partially rescue aberrant myelin decompaction in a Costello Syndrome Rasopathy model. It will be interesting to determine whether myelin alterations are present in Costello Syndrome patients, in whom many (in somatic mosaic patients) or all (in germline heterozygotes) brain cells are heterozygous for *HRAS* activating mutations. Lastly, clinical trials are ongoing in many disorders in which MAPK, NO, and Notch signals are targeted/impacted; therefore, in the case of Rasopathies, treatment trials using inhibitors of these pathways are feasible.

Acknowledgments

We are indebted to James Fagin (UTSW), Brian Popko (University of Chicago, Chicago, IL) and Tasuku Honjo (Kyoto-U) for providing mouse lines, Monica DeLay for assistance with Flow, and Merck for MRK-003. This work was supported by grants from the DOD program on Neurofibromatosis and NIH R01 NS091037 (to NR). The Cincinnati Children’s Hospital Research Foundation Flow Cytometry and Pathology Cores provided partial support for these studies (NIH P30 DK0909710551).

Bibliography

Aoki Y, Niihori T, Kawame H, Kurosawa K, Ohashi H, Tanaka Y, Filocamo M, Kato K, Suzuki Y, Kure S, et al. Germline mutations in HRAS proto-oncogene cause Costello syndrome. Nat Genet. 2005; 37:1038–40. [PubMed: 16170316]

Axelrad ME, Nicholson L, Stabley DL, Sol-Church K, Gripp KW. Longitudinal assessment of cognitive characteristics in Costello syndrome. Am J Med Genet A. 2007; 143A:3185–93. [PubMed: 17963256]

Barrett SD, Bridges AJ, Dudley DT, Saltiel AR, Fergus JH, Flamme CM, Delaney AM, Kaufman M, LePage S, Leopold WR, et al. The discovery of the benzhydroxamate MEK inhibitors CI-1040 and PD 0325901. Bioorg Med Chem Lett. 2008; 18:6501–4. [PubMed: 18952427]

Bauer NG, Richter-Landsberg C, Ffrench-Constant C. Role of the oligodendroglial cytoskeleton in differentiation and myelination. Glia. 2009; 57:1691–705. [PubMed: 19455583]

Baumgart A, Mazur PK, Anton M, Rudelius M, Schwamborn K, Feuchtinger A, Behnke K, Walch A, Braren R, Peschel C, et al. Opposing role of Notch1 and Notch2 in a Kras(G12D)-driven murine non-small cell lung cancer model. Oncogene. 2015; 34:578–88. [PubMed: 24509876]

Chen X, Mitsutake N, LaPerle K, Akeno N, Zanzonico P, Longo VA, Mitsutake S, Kimura ET, Geiger H, Santos E, et al. Endogenous expression of Hras(G12V) induces developmental defects and neoplasms with copy number imbalances of the oncogene. Proc Natl Acad Sci U S A. 2009; 106:7979–84. [PubMed: 19416908]

Colby WW, Hayflick JS, Clark SG, Levinson AD. Biochemical characterization of polypeptides encoded by mutated human Ha-ras1 genes. Mol Cell Biol. 1986; 6:730–4. [PubMed: 3537694]

Cole JS, Messing A, Trojanowski JQ, Lee VM. Modulation of axon diameter and neurofilaments by hypomyelinating Schwann cells in transgenic mice. J Neurosci. 1994; 14:6956–66. [PubMed: 7965091]

Colello RJ, Pott U, Schwab ME. The role of oligodendrocytes and myelin on axon maturation in the developing rat retinofugal pathway. J Neurosci. 1994; 14:2594–605. [PubMed: 7514208]

Cox AD, Der CJ. The dark side of Ras: regulation of apoptosis. Oncogene. 2003; 22:8999–9006. [PubMed: 14663478]

Delrue MA, Chateil JF, Arveiler B, Lacombe D. Costello syndrome and neurological abnormalities. Am J Med Genet A. 2003; 123A:301–5. [PubMed: 14608654]

Di Nicolantonio F, Arena S, Gallicchio M, Zecchin D, Martini M, Flonta SE, Stella GM, Lamba S, Cancelliere C, Russo M, et al. Replacement of normal with mutant alleles in the genome of normal human cells unveils mutation-specific drug responses. Proc Natl Acad Sci U S A. 2008; 105:20864–9. [PubMed: 19106301]

Doerflinger NH, Macklin WB, Popko B. Inducible site-specific recombination in myelinating cells. Genesis. 2003; 35:63–72. [PubMed: 12481300]

Franklin RJ, Gallo V. The translational biology of remyelination: past, present, and future. Glia. 2014; 62:1905–15. [PubMed: 24446279]

Fyffe-Maricich SL, Karlo JC, Landreth GE, Miller RH. The ERK2 mitogen-activated protein kinase regulates the timing of oligodendrocyte differentiation. J Neurosci. 2011; 31:843–50. [PubMed: 21248107]

Fyffe-Maricich SL, Schott A, Karl M, Krasno J, Miller RH. Signaling through ERK1/2 controls myelin thickness during myelin repair in the adult central nervous system. J Neurosci. 2013; 33:18402–8. [PubMed: 24259565]

Gielen E, Baron W, Vandeven M, Steels P, Hoekstra D, Ameloot M. Rafts in oligodendrocytes: evidence and structure-function relationship. Glia. 2006; 54:499–512. [PubMed: 16927294]

Gripp KW, Hopkins E, Doyle D, Dobyns WB. High incidence of progressive postnatal cerebellar enlargement in Costello syndrome: brain overgrowth associated with HRAS mutations as the likely cause of structural brain and spinal cord abnormalities. Am J Med Genet A. 2010; 152A: 1161–8. [PubMed: 20425820]

Guardiola-Diaz HM, Ishii A, Bansal R. Erk1/2 MAPK and mTOR signaling sequentially regulates progression through distinct stages of oligodendrocyte differentiation. Glia. 2012; 60:476–86. [PubMed: 22144101]

Haroutunian V, Katsel P, Roussos P, Davis KL, Altshuler LL, Bartzokis G. Myelination, oligodendrocytes, and serious mental illness. Glia. 2014; 62:1856–77. [PubMed: 25056210]

Heimfarth L, Loureiro SO, Pierozan P, de Lima BO, Reis KP, Torres EB, Pessoa-Pureur R. Methylglyoxal-induced cytotoxicity in neonatal rat brain: a role for oxidative stress and MAP kinases. Metab Brain Dis. 2013; 28:429–38. [PubMed: 23378107]

Ishii A, Furusho M, Bansal R. Sustained activation of ERK1/2 MAPK in oligodendrocytes and schwann cells enhances myelin growth and stimulates oligodendrocyte progenitor expansion. J Neurosci. 2013; 33:175–86. [PubMed: 23283332]

Jana M, Pahan K. Down-regulation of Myelin Gene Expression in Human Oligodendrocytes by Nitric Oxide: Implications for Demyelination in Multiple Sclerosis. J Clin Cell Immunol. 2013; 4

Kalyanaraman B, Darley-Usmar V, Davies KJ, Dennery PA, Forman HJ, Grisham MB, Mann GE, Moore K, Roberts LJ 2nd, Ischiropoulos H. Measuring reactive oxygen and nitrogen species with fluorescent probes: challenges and limitations. Free Radic Biol Med. 2012; 52:1–6. [PubMed: 22027063]

Koenning M, Jackson S, Hay CM, Faux C, Kilpatrick TJ, Willingham M, Emery B. Myelin gene regulatory factor is required for maintenance of myelin and mature oligodendrocyte identity in the adult CNS. J Neurosci. 2012; 32:12528–42. [PubMed: 22956843]

Krencik R, Hokanson KC, Narayan AR, Dvornik J, Rooney GE, Rauen KA, Weiss LA, Rowitch DH, Ullian EM. Dysregulation of astrocyte extracellular signaling in Costello syndrome. Sci Transl Med. 2015; 7:286ra66.

Langosch D, Scharnagl C, Steiner H, Lemberg MK. Understanding intramembrane proteolysis: from protein dynamics to reaction kinetics. Trends Biochem Sci. 2015; 40:318–27. [PubMed: 25941170]

Lewis HD, Leveridge M, Strack PR, Haldon CD, O'Neil J, Kim H, Madin A, Hannam JC, Look AT, Kohl N, et al. Apoptosis in T cell acute lymphoblastic leukemia cells after cell cycle arrest induced by pharmacological inhibition of notch signaling. Chem Biol. 2007; 14:209–19. [PubMed: 17317574]

Li S, Vana AC, Ribeiro R, Zhang Y. Distinct role of nitric oxide and peroxynitrite in mediating oligodendrocyte toxicity in culture and in experimental autoimmune encephalomyelitis. Neuroscience. 2011; 184:107–19. [PubMed: 21511012]

López-Juárez A, Titus HE, Silbak S, Pressler JW, Rizvi TA, Bogard M, Bennett MR, Williams MT, Vorhees CV, Ratner N. Oligodendrocyte Nf1 Controls Aberrant Notch Activation and Regulates Myelin Structure and Behavior. Cell reports. 2017; 9:545–557.

Mainberger F, Langer S, Mall V, Jung NH. Impaired synaptic plasticity in RASopathies: a mini-review. J Neural Transm (Vienna). 2016; 123:1133–8. [PubMed: 27565148]

Martini R, Schachner M. Molecular bases of myelin formation as revealed by investigations on mice deficient in glial cell surface molecules. Glia. 1997; 19:298–310. [PubMed: 9097074]

Mayes DA, Rizvi TA, Titus-Mitchell H, Oberst R, Ciraolo GM, Vorhees CV, Robinson AP, Miller SD, Cancelas JA, Stemmer-Rachamimov AO, et al. Nf1 loss and Ras hyperactivation in oligodendrocytes induce NOS-driven defects in myelin and vasculature. Cell Rep. 2013; 4:1197–212. [PubMed: 24035394]

Quezada E, Gripp KW. Costello syndrome and related disorders. Curr Opin Pediatr. 2007; 19:636–44. [PubMed: 18025929]

Quinlan MP, Quatela SE, Philips MR, Settleman J. Activated Kras, but not Hras or Nras, may initiate tumors of endodermal origin via stem cell expansion. Mol Cell Biol. 2008; 28:2659–74. [PubMed: 18268007]

Rauch N, Rukhlenko OS, Kolch W, Kholodenko BN. MAPK kinase signalling dynamics regulate cell fate decisions and drug resistance. Curr Opin Struct Biol. 2016; 41:151–158. [PubMed: 27521656]

Rauen KA. HRAS and the Costello syndrome. Clin Genet. 2007; 71:101–8. [PubMed: 17250658]

Robinson AP, Rodgers JM, Goings GE, Miller SD. Characterization of oligodendroglial populations in mouse demyelinating disease using flow cytometry: clues for MS pathogenesis. PLoS One. 2014; 9:e107649. [PubMed: 25247590]

Rooney GE, Goodwin AF, Depeille P, Sharir A, Schofield CM, Yeh E, Roose JP, Klein OD, Rauen KA, Weiss LA, et al. Human iPS Cell-Derived Neurons Uncover the Impact of Increased Ras Signaling in Costello Syndrome. J Neurosci. 2016; 36:142–52. [PubMed: 26740656]

Sarkisian CJ, Keister BA, Stairs DB, Boxer RB, Moody SE, Chodosh LA. Dose-dependent oncogene-induced senescence in vivo and its evasion during mammary tumorigenesis. Nat Cell Biol. 2007; 9:493–505. [PubMed: 17450133]

Serrano M, Lin AW, McCurrach ME, Beach D, Lowe SW. Oncogenic ras provokes premature cell senescence associated with accumulation of p53 and p16INK4a. Cell. 1997; 88:593–602. [PubMed: 9054499]

Sparey T, Beher D, Best J, Biba M, Castro JL, Clarke E, Hannam J, Harrison T, Lewis H, Madin A, et al. Cyclic sulfamide gamma-secretase inhibitors. Bioorg Med Chem Lett. 2005; 15:4212–6. [PubMed: 16054361]

Sundaram MV. The love-hate relationship between Ras and Notch. Genes Dev. 2005; 19:1825–39. [PubMed: 16103211]

Tidyman WE, Rauen KA. Pathogenetics of the RASopathies. Hum Mol Genet. 2016; 25:R123–R132. [PubMed: 27412009]

To MD, Wong CE, Karnezis AN, Del Rosario R, Di Lauro R, Balmain A. Kras regulatory elements and exon 4A determine mutation specificity in lung cancer. Nat Genet. 2008; 40:1240–4. [PubMed: 18758463]

Wang S, Sdrulla AD, diSibio G, Bush G, Nofziger D, Hicks C, Weinmaster G, Barres BA. Notch receptor activation inhibits oligodendrocyte differentiation. Neuron. 1998; 21:63–75. [PubMed: 9697852]

Watkins TA, Emery B, Mulinyawe S, Barres BA. Distinct stages of myelination regulated by gamma-secretase and astrocytes in a rapidly myelinating CNS coculture system. Neuron. 2008; 60:555–69. [PubMed: 19038214]

Xiao L, Guo D, Hu C, Shen W, Shan L, Li C, Liu X, Yang W, Zhang W, He C. Diosgenin promotes oligodendrocyte progenitor cell differentiation through estrogen receptor-mediated ERK1/2 activation to accelerate remyelination. Glia. 2012; 60:1037–52. [PubMed: 22461009]

Zampino G, Pantaleoni F, Carta C, Cobellis G, Vasta I, Neri C, Pogna EA, De Feo E, Delogu A, Sarkozy A, et al. Diversity, parental germline origin, and phenotypic spectrum of de novo HRAS missense changes in Costello syndrome. Hum Mutat. 2007; 28:265–72. [PubMed: 17054105]

Main Points

- In a Costello syndrome model, *HRasG12V* expression in mature oligodendrocytes activates the MAPK pathway, causing myelin decompaction.
- Combining inhibition of any two pathways, of MAPK, Nitric Oxide and Notch signaling, rescues myelin defects.

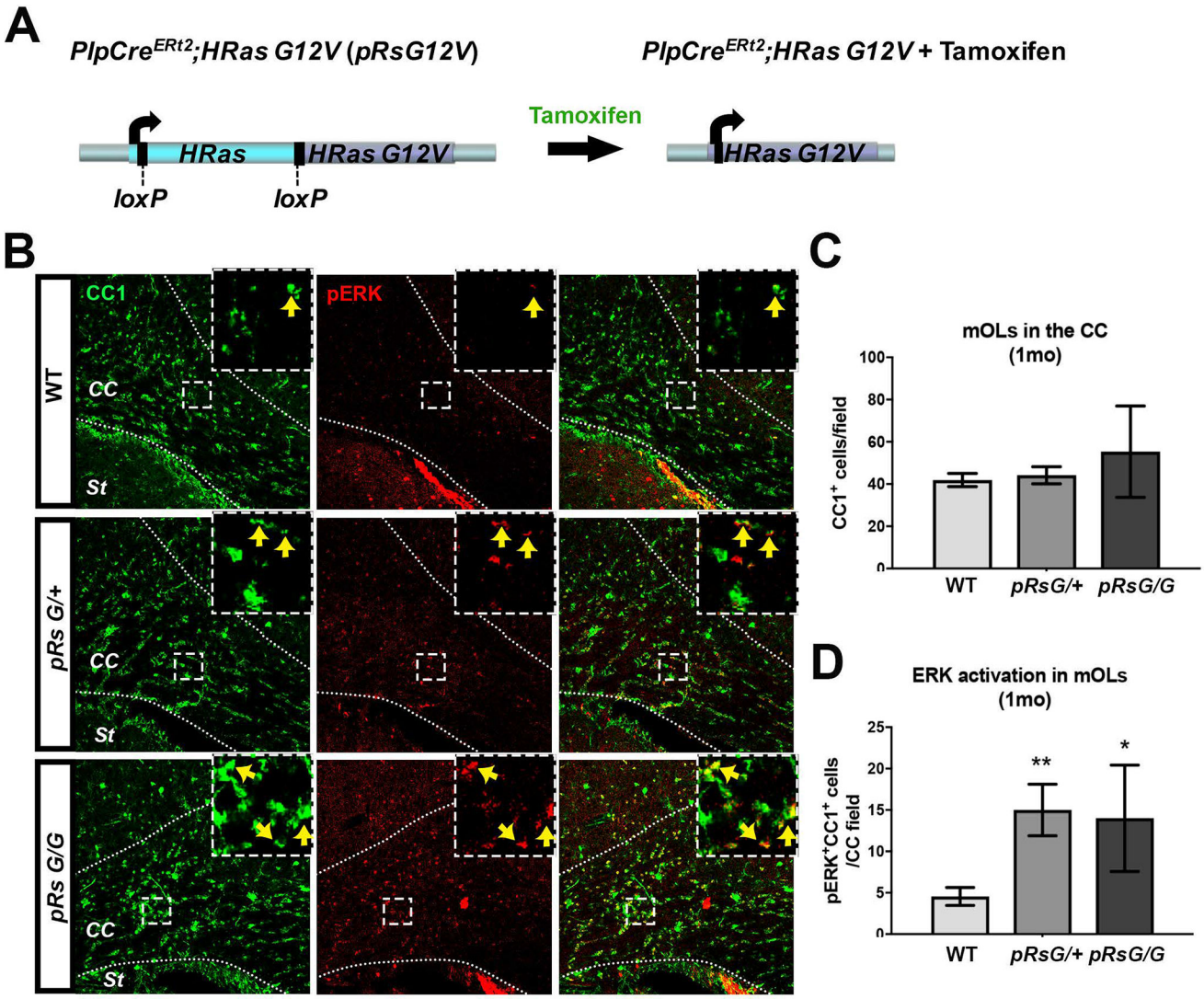

FIGURE 1. *RasG12V* mutation in mature oligodendrocytes activates MAPK pathway without affecting oligodendrocyte numbers

A: Schematic representation of the genomic region containing the endogenous *HRas* gene in *PlpCre^{ERt2};HRasG12V* mice (*pRsG12V*). Left: the WT *HRas* gene (cyan) flanked by *loxP* sites [exons 1–4 (Chen et al. 2009)] is localized upstream of the mutant *HRasG12V* gene (purple). Right: following tamoxifen administration, active Cre recombinase mediates the excision of WT *HRas*, allowing the expression of the mutant *HRasG12V* allele from the *HRas* locus. The mutant allele is not expressed unless the WT copy is excised. B: Corpus callosum (CC) of WT mice (top), hemizygous (middle), and homozygous (bottom) *pRsG12V* mutants, one month (1mo) after tamoxifen treatment showing staining for the marker of mature oligodendrocytes CC1 (green), the phosphorylated form of ERK (pERK, red), and overlap (right column). Positive cells for both markers are indicated with arrows within the insets from the squared areas. St: striatum. C: Quantification of CC1$^+$ cells indicates no differences in the number of oligodendrocytes in *pRsG/+* (n= 6 mice, unpaired *t* test, p=0.66) or *pRsG/G* (n= 3 mice, unpaired *t* test, p=0.31) mutants, as compared to WT mice (n= 9 mice). D: Quantification of CC1$^+$;pERK$^+$ cells indicates significantly increased

ERK activation in oligodendrocytes of *pRsG/+* (n= 6 mice, unpaired *t* test, **p=0.002) or *pRsG/G* (n= 3 mice, unpaired *t* test, *p=0.034) mutants, as compared to WT mice (n= 9 mice). All data are presented as the mean ± s.e.m.

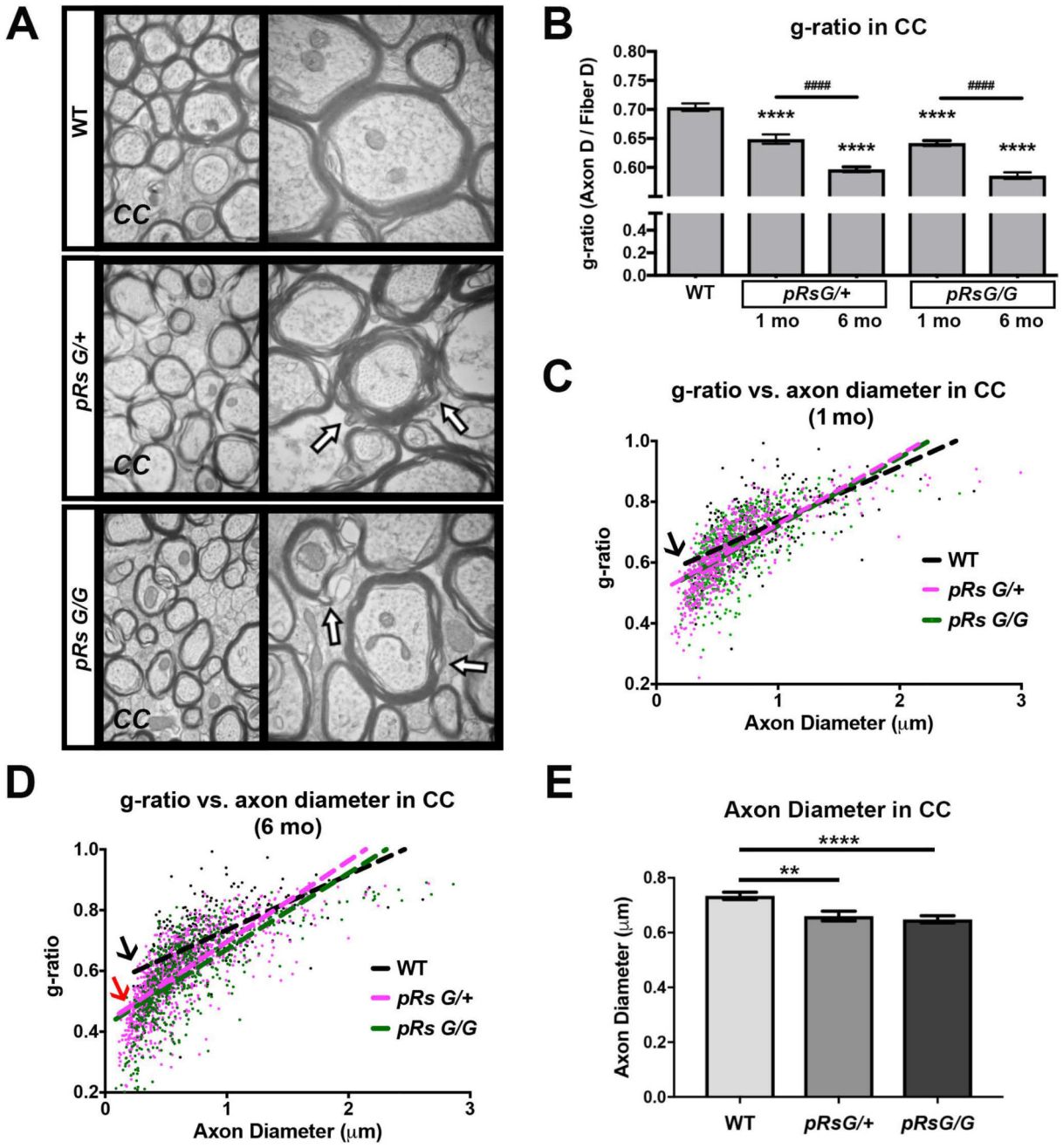

FIGURE 2. ***HRas*** **hyperactivation in mature oligodendrocytes decreases g-ratio**

A: Electron micrographs of myelinated axons in the corpus callosum (CC) at the midline of WT, *pRsG/+*, and *pRsG/G* mice 1 month after tamoxifen treatment. High magnifications (50,000×) are shown at right; regions with myelin decompaction (See also figure 3A) are indicated with arrows. B: Analysis of only myelinated axons indicates decreased g-ratio in *pRsG/+* and *pRsG/G* mutants at 1 month (1mo, n= 3 mice per genotype) and 6 months (6mo, *pRsG/+* mice; n= 5, *pRsG/G* mice; n= 3 mice) post-tamoxifen (****p<0.0001), as compared to g-ratio in WT mice (n= 6 mice). The g-ratio was further decreased in *pRsG/+* and *pRsG/G* mutants at 6 months post-tamoxifen, as compared to *pRsG/+* and *pRsG/G* mice 1 month

after tamoxifen (####p<0.0001), respectively. C–D: Scatterplots and linear regression of the axon diameter vs. g-ratio from myelinated fibers in WT (black), *pRsG/+* (pink), and *pRsG*/G (green) mice, 1 month (C) and 6 months (D) after tamoxifen treatment. The slopes of g-ratio vs. axon diameter are similar in *HRas* mutants compared to WT mice at 1 mo (C, black arrow); however, small g-ratio in *HRas* mutants is associated to small diameter axons at 6 mo (D, black arrow vs. red arrow). E: Evaluation of the diameter of myelinated axons shows significant decreases in *pRsG/+* (n= 3 mice, **p=0.001) and *pRsG/G* (n= 3 mice, ****p<0.0001) 1 month after tamoxifen treatment, as compared to WT mice. One way ANOVA and Tukey's multiple comparisons test was used in the analyses. All data are presented as the mean ± s.e.m.

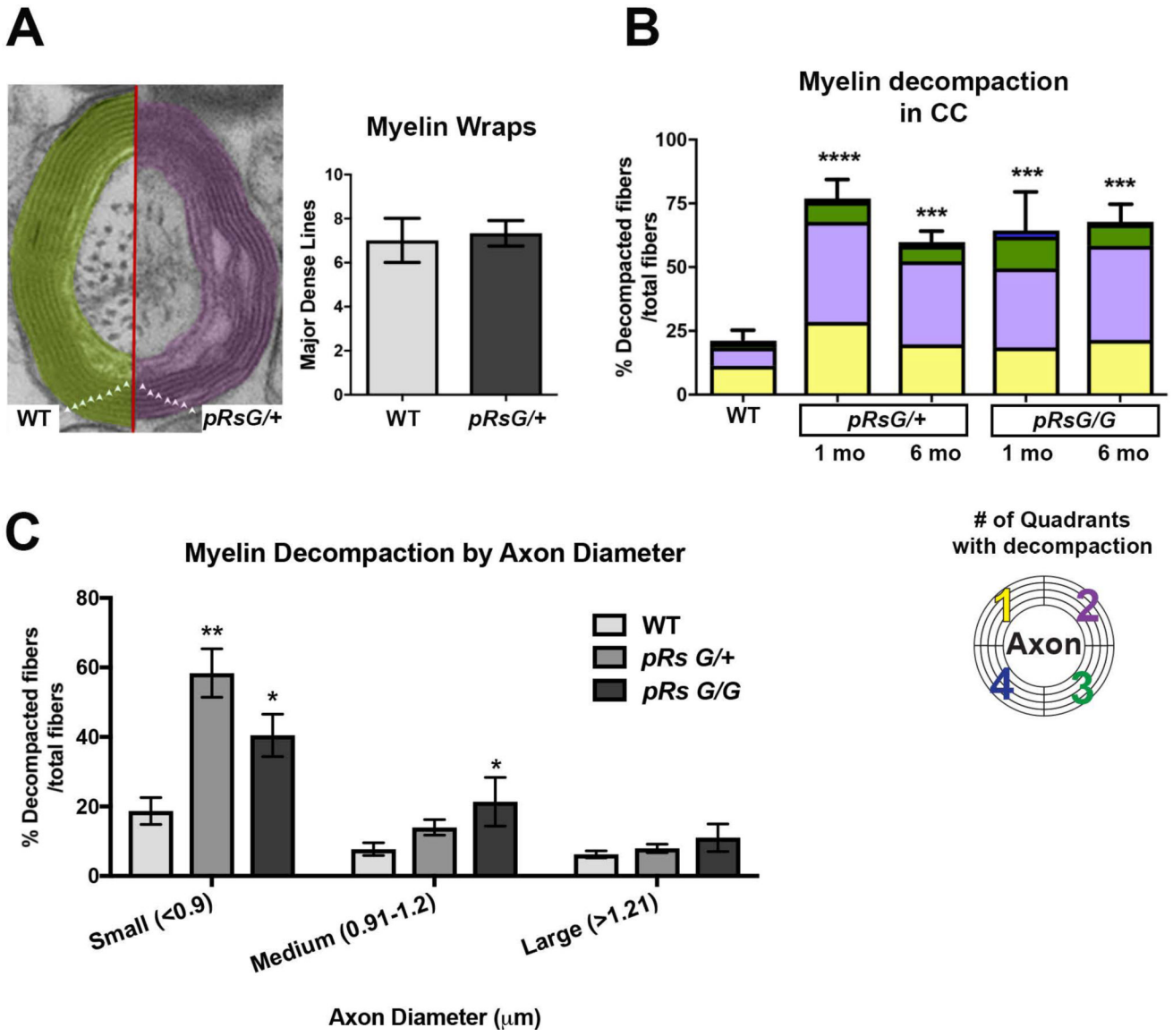

FIGURE 3. ***HRas*** **hyperactivation in mature oligodendrocytes causes myelin decompaction**

A: Left: Representative image of the number of myelin lamellae (triangles) wrapping an axon in WT and *pRsG/+* mice. Right: quantitative analysis indicates no significant changes in the number of myelin wraps between WT and *pRsG/+* mice (unpaired *t* test, p=0.64). B: Analysis of myelinated axons indicates significantly increased percent of fibers with myelin decompaction in *pRsG/+* mutants at 1 month (1 mo, n= 3 mice, ****p=0.0001) and 6 months (6 mo, n= 5 mice, ***p=0.0006) post-tamoxifen, compared to WT mice (n= 3 mice). Myelin decompaction was also observed in *pRsG/G* mutants at 1 mo (n= 3 mice, ***p=0.0009) and 6 mo (n= 3 mice, ***p=0.0005) post-tamoxifen, as compared to WT mice. No significant changes were observed among different time points in both *pRsG12V* mutants. The percent of fibers showing decompaction in 1–4 quadrants (color code; bottom) is shown within the total fibers with decompaction, as a reference for severity of the phenotype. C: Significantly increased percent of decompacted myelin was detected in fibers containing small axons (<0.9 μm, n= 3 mice, **p=0.001) in *pRsG/+* mutants, and small (n=

3 mice, *p=0.037) and medium (0.91–1.2 μm, n= 3 mice, *p=0.048) axons of in *pRsG/G* mutants 1 month post-tamoxifen, as compared to WT mice (n= 6 mice). One way ANOVA and Tukey's multiple comparisons test was used in all analyses, except in panel A (Student's *t* test). All data are presented as the mean ± s.e.m.

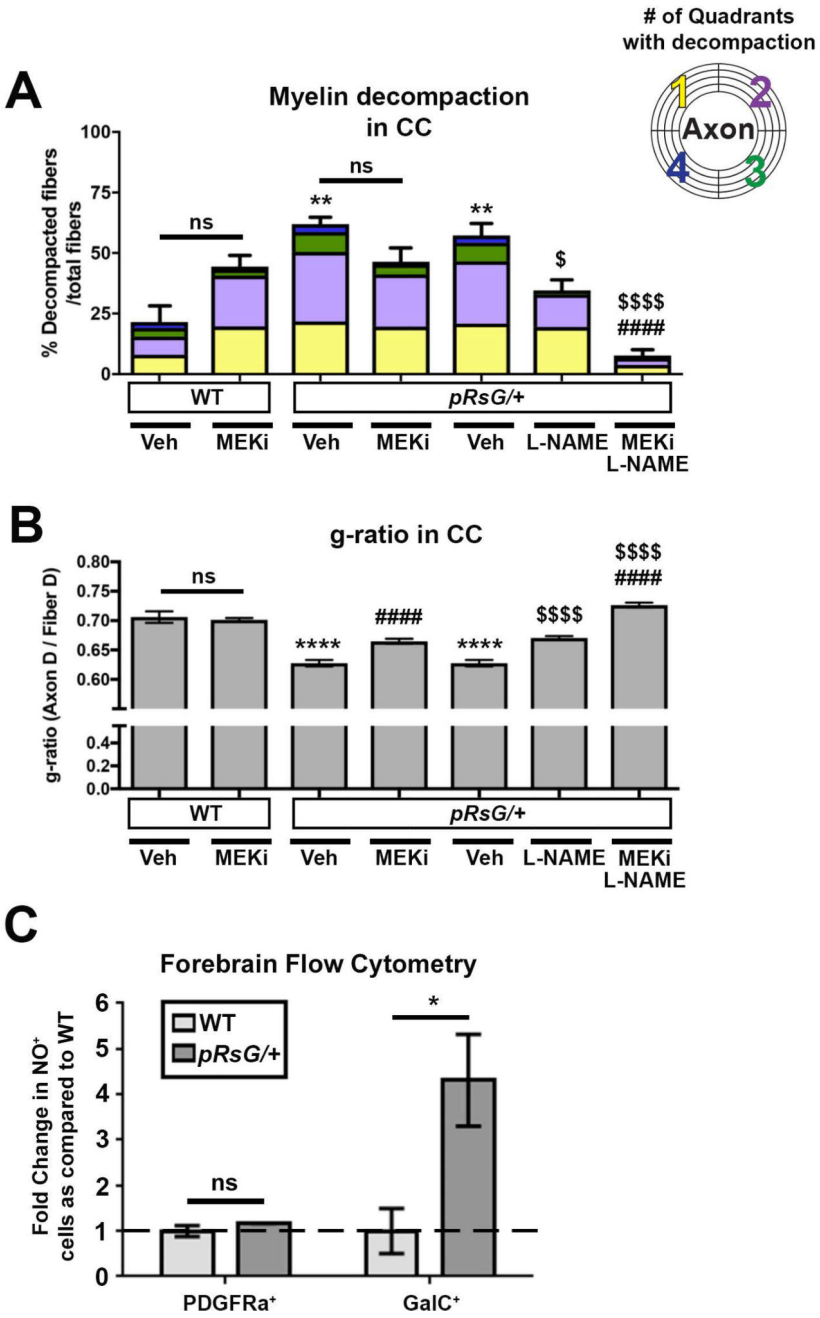

FIGURE 4. Myelin defects in *pRsG/+* mutants are susceptible to MEK and NOS pharmacological inhibition

A: Quantification of total fibers with myelin decompaction, and quadrants with decompaction (color code), in WT and *pRsG/+* mutants subjected to the indicated pharmacological treatments 1 month post-tamoxifen. No significant changes (but a trend toward increase) are observed in the percent of decompacted fibers in MEK inhibitor (MEKi)-treated WT (n= 6), as compared to vehicle-treated WT mice (n= 3, ns: not significant, p=0.219). Vehicle-treated *pRsG/+* mutants (n= 3) show increased myelin decompaction, as compared to vehicle-treated WT mice (methocel for MEKi; **p=0.002 and PBS for L-NAME; **p=0.003). No significant changes (but a trend toward decrease)

were observed in decompaction in *pRsG/+* mutants treated with MEKi (n= 3 mice), as compared to vehicle-treated mutants (ns, p=0.261). Significantly decreased percent of decompacted fibers were observed in *pRsG/+* mutants treated with L-NAME (n= 4 mice, $^{\$}$p=0.030), and myelin compaction was fully rescued to WT levels by concomitant treatment with L-NAME and MEKi, as compared to vehicle-treated mutants (n= 4 mice, $^{\#\#\#\#,\$\$\$\$}$p<.0001). B: The g-ratio comparison of WT and *pRsG/+* mutants subjected to the indicated pharmacological treatments 1 month post-tamoxifen (same cohort of mice as in panel A). No significant changes were observed in g-ratio of vehicle-treated *vs.* MEKi-treated WT mice (ns, p=0.996). Vehicle-treated *pRsG/+* mutants show decreased g-ratio, as compared to WT mice (PBS or methocel ****p<0.0001). Significantly increased g-ratio was observed in *pRsG/+* mutants treated with MEKi ($^{\#\#\#\#}$p<0.0001) or L-NAME ($^{\$\$\$\$}$p<0.0001), as compared to vehicle-treated mutants, respectively. Furthermore, increased g-ratio was observed in *pRsG/+* mutants concomitantly treated with MEK and L-NAME ($^{\#\#\#\#,\$\$\$\$}$p<0.0001). C: Flow cytometry analysis of forebrain cells indicates no change in the number of PDGFRa^{+} OL precursors showing Nitric Oxide (NO) signals (ns, p=0.225); however, the number of GalC^{+};NO^{+} mOLs are significantly increased in *pRsG/+* mutants (n= 3 mice, *t* test, *p=0.042), as compared to WT mice (n= 3 mice). Data are presented as the mean ± s.e.m. One-way ANOVA and Tukey's multiple comparisons test were used in all panels, except in C.

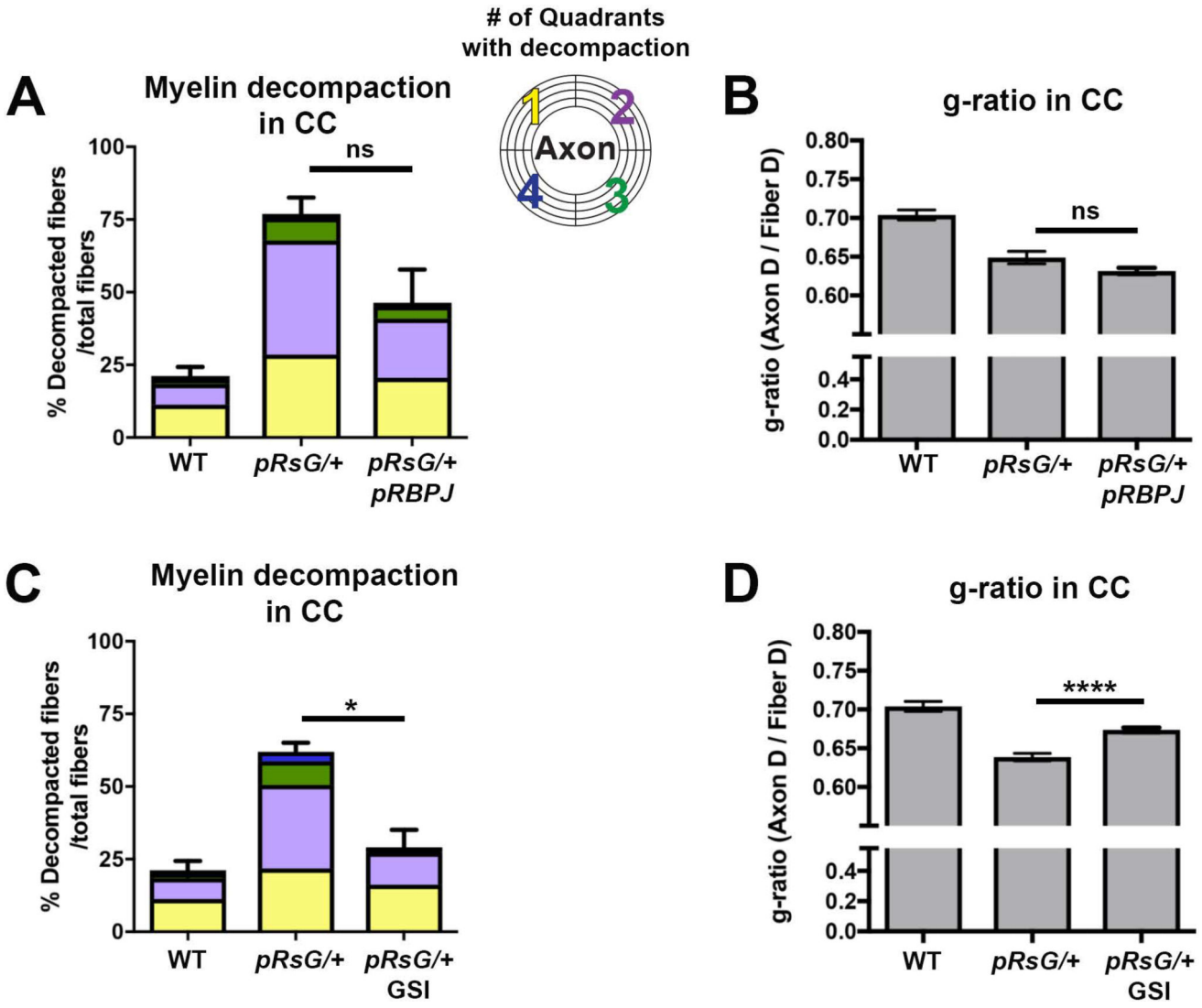

FIGURE 5. Effects of Notch signaling inhibition on myelin defects in *HRasG12V* mutants

Quantification of total fibers with myelin decompaction and quadrants with decompaction (panels A and C), and g-ratio evaluation (panels B and D), in WT (n= 6 mice), *pRsG/+* (n= 3 mice), *pRsG/+;pRBPJ* (n= 5 mice), and GSI-treated *pRsG/+* (n= 6 mice) mice, 1 month post-tamoxifen. A: No significant changes (but a trend toward decrease) were observed in the percent of decompacted fibers in *pRsG/+;pRBPJ* mutants, as compared to *pRsG/+* mice (ns, p=0.091). B: No significant changes were observed in the g-ratio of *pRsG/+;pRBPJ* mutants, as compared to *pRsG/+* mice (ns, p=0.086). C: Significantly decreased percent of decompacted fibers was observed in GSI-treated *pRsG/+* mutants, as compared to vehicle-treated *pRsG/+* mice (*p=0.011). D: A significant increase in g-ratio was detected in GSI-treated mutants, as compared to *pRsG/+* mice (ns, p<0.0001). In all panels; WT values are shown for reference, One-way ANOVA and Tukey's multiple comparisons test were used, and data are presented as the mean ± s.e.m.

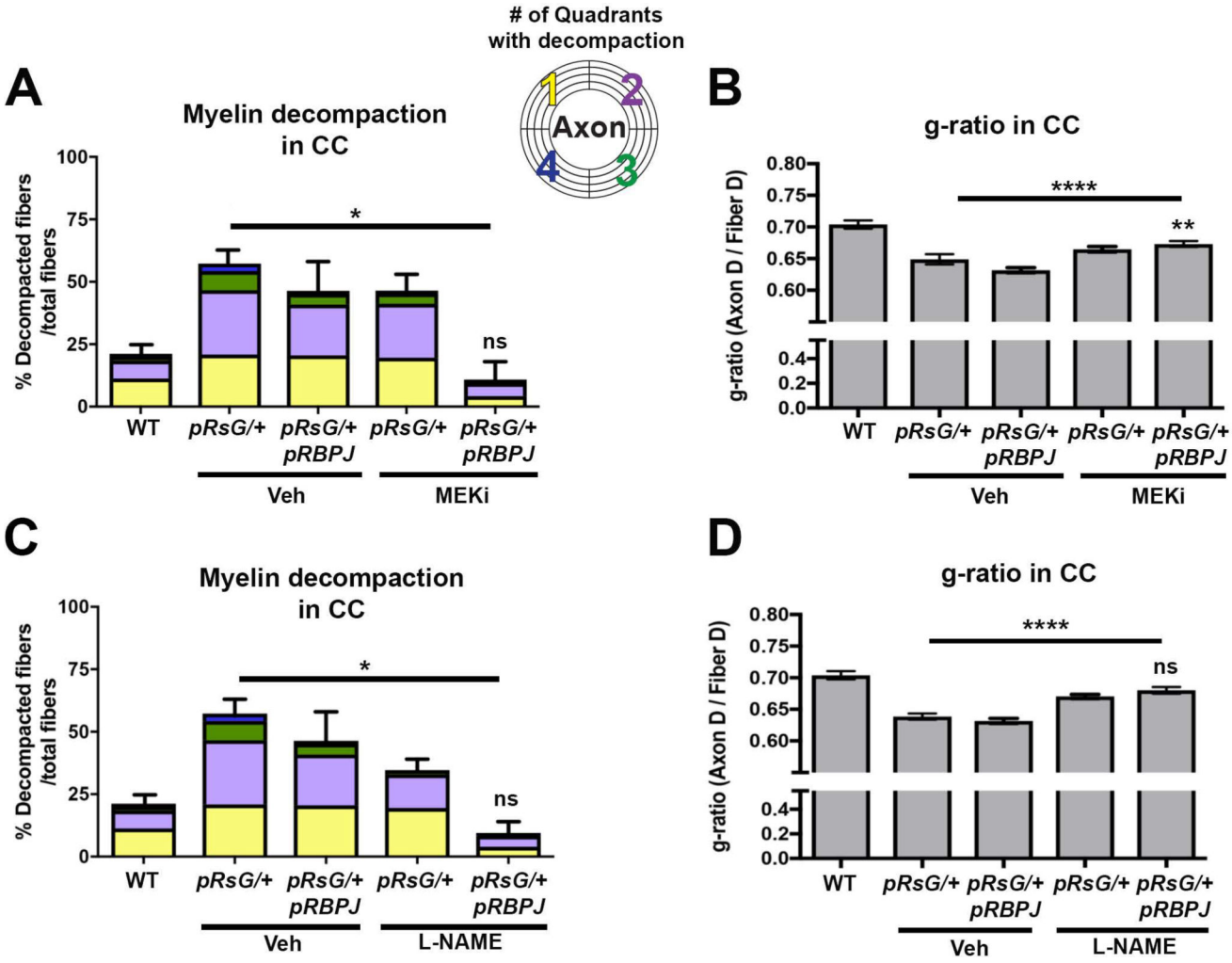

FIGURE 6. Concomitant inactivation of *RBPJ* and MEK or NOS pharmacological inactivation fully rescues myelin abnormalities in *HRasG12V* mutants

Quantification of total fibers with myelin decompaction and quadrants with decompaction (panels A and C), as well as g-ratio evaluation (panels B and D), in WT, *pRsG/+*, and *pRsG/+;pRBPJf/f* mice treated with vehicle, MEKi, or L-NAME, 1 month post-tamoxifen. A: Full rescue of myelin compaction to WT levels (WT; n= 6 mice, p=0.938) was observed in *pRsG/+;pRBPJf/f* mice treated with MEKi (n= 3 mice), as compared to *pRsG/+* mice (n= 4 mice, *p=0.031). B) The g-ratio was significantly increased in MEKi-treated *pRsG/+;pRBPJf/f* mutants, as compared to vehicle-treated *pRsG/+* mice (****p<0.0001); however, the g-ratio was still significantly lower than those in WT mice (**p=0.007). C: Significantly decreased myelin decompaction was observed in *pRsG/+;pRBPJf/f* mice treated with L-NAME (n= 3 mice), as compared to *pRsG/+* mice (n= 6 mice, *p=0.021), and the values of decompaction were not significantly different than those of WT mice (ns, p=0.888). D) The g-ratio was significantly increased in L-NAME-treated *pRsG/+;pRBPJf/f* mutants, as compared to vehicle-treated *pRsG/+* mice (****p<0.0001), and g-ratio was not different from those of WT mice (ns, p=0.057). In all panels, One-way ANOVA and Tukey's multiple comparisons test was used and data are presented as the mean ± s.e.m.

Table 1

Mouse strains used in this study

Genotype	Description	Abbreviation	Reference
B6.Cg-Tg(Plp1-Cre/ERT)3Pop/J	Tamoxifen Inducible Cre recombinase under the transcriptional control of the mOL marker Plp1	*PlpCre^{ER}*	Doerflinger et al., 2003
FR-Hras^{G12V}	Mutant HRasG12V allele upstream of WT HRas flanked by loxP sites	*HRas^{G12V}*	Chen et al., 2009
RBP-J^{flox}	Endogenous rbpj gene flanked by loxP sites	*Rbpj^{flox}*	Han et al., 2002
B6.Cg-Tg(Plp1-Cre/ERT)3Pop/J; FR-HrasG12V	Tamoxifen administration mediates excision of endogenous (WT) *HRas* and expression of the mutant *HRasG12V* allele.	*pRsG/+* or *pRsG/G*	--
*B6.Cg-Tg(Plp1-Cre/ERT)3Pop/J; FR-HrasG12V;*RBP-J^{flox}	Tamoxifen administration mediates excision of endogenous (WT) *HRas*, expression of the mutant *HRasG12V* allele and inactivation of *Rbpj*.	*pRsG/+;pRbpj*	--